Hidden Role of a Hydroxyl Group in Mediating the Oxygen Line Defect on a Graphene Surface

ARTICLE *in* THE JOURNAL OF PHYSICAL CHEMISTRY C · AUGUST 2013

Impact Factor: 4.77 · DOI: 10.1021/jp4052159

3 AUTHORS:

Hongguang Liu
Jinan University (Guangzhou, China)
16 PUBLICATIONS **200** CITATIONS
SEE PROFILE

Baotao Kang
Sungkyunkwan University
16 PUBLICATIONS **94** CITATIONS
SEE PROFILE

Jai Young Lee
Konyang University
101 PUBLICATIONS **970** CITATIONS
SEE PROFILE

THE JOURNAL OF PHYSICAL CHEMISTRY C

Article

pubs.acs.org/JPCC

Hidden Role of a Hydroxyl Group in Mediating the Oxygen Line Defect on a Graphene Surface

Hongguang Liu, Baotao Kang, and Jin Yong Lee*

Department of Chemistry, Sungkyunkwan University, Suwon 440-746, Korea

ABSTRACT: Atomic fault lines stemming from the linear assembly of epoxy groups are recently proposed to be responsible for the decrease of bulk size of graphitic materials. Yet, the formation of such a line by either the hopping of existing epoxides or the binding with environmental atomic oxygens seems to be infeasible. By employing both finite and periodic graphene models, we uncovered the role of hydroxyl, which is essentially ignored in previous reports, in mediating the epoxy line. It is noteworthy that the intercalation of OH impedes the unzipping of underlying carbons and induces a smoother surface buckling along the epoxy line. The fault line formation would be ascribed to the creation of vacancies when the system temperature elevates.

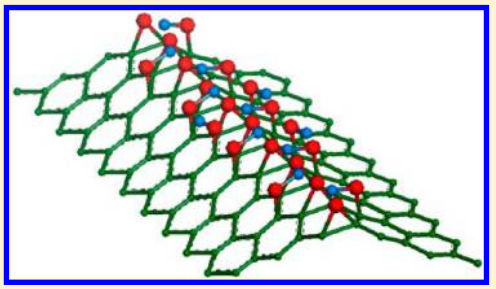

INTRODUCTION

Carbon allotropes (graphite, diamond, and carbon black) and especially graphene have received enormous scientific interest because of their fascinating physical, mechanical, and electrical properties.[1−13] Chemical oxidation of graphite followed by exfoliation in solution allows a large-scale production of isolated graphene oxide (GO). So far quite a number of work in the experimental literature regarding the chemistry of GO has provided preliminary knowledge of the average oxidation level[14,15] and the diversity of oxygen groups,[16] while comparatively little has been done to link oxidation chemistry with the morphology of the atomically thin graphene. In a pioneering study, Li et al.[17] provided optical microscope images of the graphite surface to evidently reveal the formation of fault lines owing to the oxidative process. By means of first-principles quantum mechanical calculations, they first explained that it is a cooperative alignment of epoxy groups that leads to the carbon lattice unzipping. This investigation is very enlightening because, first, the epoxy lines on GO might be responsible for their much smaller size compared with the starting graphite materials during oxidation[18] or later thermal reduction,[16,19] and, second, the existence of uniformly aligned epoxy groups may also shed light on the wrinkled nature of graphene monolayers, because graphene surface bucklings are easily induced by kink lines consisting of functional groups.[20]

So far so good, but how easily do the randomly bound epoxy groups align themselves and trigger the breakup of the underlying carbon lattice? The authors of reference 17 employed two graphene models ($C_{24}H_{12}$ and $C_{54}H_{18}$) to exploit the low level oxidation process, and the results indicated that the linear oxygen clustering is thermally favored but kinetically difficult. Meanwhile, Ajayan et al.[18] also pointed out that the epoxy groups can only line up as a result of rapid hoppings, but high energy barriers needed to be overcome. The mismatch forces us to question if there are there any essential factors that are ignored in this process.

Numerous studies have pointed to the fact that the basal plane of GO is covered with mostly epoxide and hydroxyl functionalities.[16,19,21,22] Then taking into account the experimental observation of Cai et al.[22] who found that a large fraction of C−epoxide and C−OH are bonded to each other on the GO surface, we thus start to speculate whether the hydroxyl groups (OH) contribute to facilitate the process of linear oxygen clustering. Our speculation was also inspired by another experimental fact that the ordered oxygen alignment on the graphene surface is not observed under the environment of atomic oxygens (without H) even if the oxygen dose is increased.[23]

The defective structures and dynamics of carbon-based nanomaterials were discussed mostly from the theoretical point of view throughtout the literature, due to a lack of suitable techniques to adequately access these areas.[24−27] To computationally study the presented idea, we employed both finite and periodic graphene models to probe the role of OH in assisting the linear oxygen assembly.

COMPUTATION METHODS

Hitherto many research works have utilized graphene flake to approximate surface reaction that took place on graphene.[28−30] For the finite graphene model, a flake ($C_{80}H_{22}$) which is larger than that simulated in ref 17 was constructed. Density functional theory (DFT) calculations were performed with the program Gaussian 09,[31] using the dispersion-corrected M06-2X functional and 6-31g(d) basis set. Among the tested hybrid meta exchange-correlation functionals, M06-2X provides the best results for the combination of main-group thermochemistry, kinetics and noncovalent interactions.[32,33] The integral=ultrafine option was implemented to minimize the

Received: May 27, 2013
Revised: July 26, 2013
Published: August 1, 2013

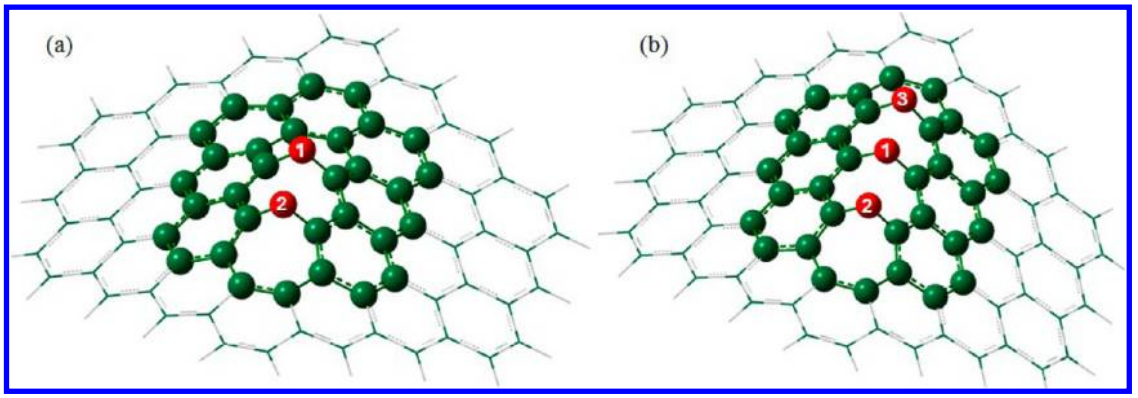

Figure 1. Unzipped structures with two (a) or three (b) epoxy groups on $C_{80}H_{22}$. The numbering implies the sequential incorporation of the epoxy group.

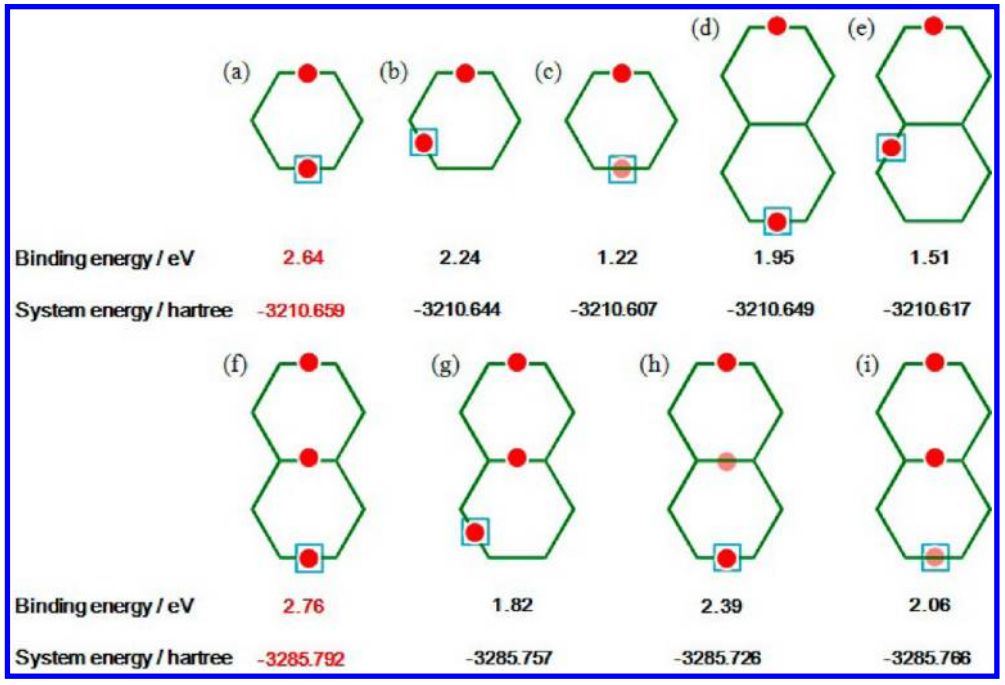

Figure 2. Binding energies of specified epoxides and system energies of tested configurations. The binding of subsequent O is specified by a blue square and the transparent red ball indicates that the epoxy group locates at the opposite side of the $C_{80}H_{22}$ sheet. To note, the binding of oxygen species (including OH) investigated in this study is exothermic. Throughout the context, the absolute value of the binding energy is utilized.

integration grid errors that may arise from employing an inadequate grid in the current M06 suite of functionals,[34] though the default grid (i.e., fine grid) in Gaussian 09 is sufficient. All molecular structures were allowed to fully relax. We computed the restricted/unrestricted singlet states and triplet state of $C_{80}H_{22}$; no open-shell properties were found. The close-shell singlet state could be recognized as the electronic ground state. Frequency calculations were carried out at the same level of theory to identify all of stationary points as minima (zero imaginary frequencies) or first-order saddle points (one imaginary frequency). An intrinsic reaction coordinate (IRC) calculation was performed to verify that the optimized geometry to be used was in fact a transition state. Zero-point corrected energies were used throughout the calculations. We have shown in previous work[35] that this model system can predict the oxygen site-to-site hopping barrier (36.4 kcal/mol) with sufficient accuracy which is in good agreement with the experimental data (35 kcal/mol).[36] For comparison, we also computed the barrier at the level of B3LYP/6-31g(d), yielding a value of 25.4 kcal/mol which is numerically close to ca. 20.8 kcal/mol reported in ref 17. The origin of the energy difference between different methods has been discussed elsewhere,[35] but these comparisons suggest that our model at the level of M06-2X/6-31g(d) is sufficient for an approximate analysis of the energetics of oxygen surface arrangements. To obtain the energy in the presence of solvent, we performed full optimization rather than single-point calculation using the polarizable continuum model[37] (PCM) implemented in Gaussian 09. Two kinds of solvents, water and dimethylformamide, were considered since they were reported experimentally that they could accelerate the diffusion of oxygen groups of dispersed GO.[38]

The graphene model under periodic boundary conditions (PBCs) was simulated in DMol3 code[39] to address the internal similarities and discrepancies between the graphene nanoflake and the larger graphene. The calculations were carried out by DFT with the revised Perdew–Burke–Ernzerhof (RPBE) functional[40] as implemented in DMol3 code. The lattice

dx.doi.org/10.1021/jp4052159 | J. Phys. Chem. C 2013, 117, 17832–17838

constants of graphene were first fully optimized with a 20 Å vacuum space. During calculations, all electron treatment was performed and a double numerical plus polarization (DNP) was used as the basis set. The convergence tolerance of energy was taken as 10^{-5} hartree, and the maximum allowed force and displacement were 0.002 hartree·Å^{-1} and 0.005 Å, respectively. A supercell of 7 ×7 × 1 was investigated with Brillouin zone *k*-point meshes of 4 × 4 × 1. Transition state calculations were performed by the LST/QST method.[41]

RESULTS AND DISCUSSION

The optimum configuration when an oxygen atom binds to the honeycomb carbon lattice is in the epoxide form. In the equilibrium state, the underlying C−C bond is stretched to 1.55 Å, in reasonable agreement with previous theoretical results[17,42] and indicating no structure unzipping. When the second epoxide is incorporated to the flake, the bond unzipping is initiated by two epoxides aligned parallel on the same carbon hexagon and the same side of the sheet (Figure 1a). The breakup of underlying C−C bonds releases the strain caused by epoxy bridges, and in return stabilizes the epoxides and extends the existing unzipping (Figure 1b). On the other hand, the one-side epoxy line buckles the carbon sheet along the same direction which may be another driving force to fracture the C−C bond. The binding of the second (the third) O is stronger than that of the first one by 1.24 (1.35) eV in energy suggesting the linear assembly of epoxides are thermally preferential. Despite these special clusterings, other possibilities were also considered (Figure 2). It is straightforward that the one-side linear mode has the largest O binding energy and its system energy is lower than that of the other tested configurations. We also found surface buckling induced by the existing epoxide is offset by the epoxy group at the opposite side of the graphene sheet, which as a result terminates the unzipping and makes the carbon lattice severely strained. Our results point to the notion that the formation of an epoxy line on the graphene sheet is more likely to be a one-side property.

Figure 3 shows the energy barriers for the O migration between two nearest bonding sites. It is clear that R_1 has a relatively lower barrier than R_2 in both dimer and trimer cases. Although the barriers of R_1 in Figure 3b and 3c are exclusively lower than that of the isolated epoxide site-to-site hopping, the barrier is still high; hence we cannot say the subsequent oxygen chain reaction is kinetically favored. Especially the unzipped epoxide dimer does not facilitate the third O jumping along R_1.

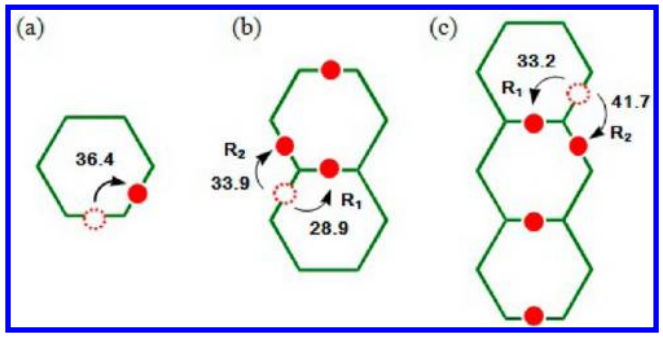

Figure 3. Oxygen hopping barriers between two nearest bonding sites in the cases of isolated epoxide (a), epoxide dimer (b), and epoxide trimer (c) on $C_{80}H_{22}$. R_1 and R_2 refer to two different hopping routes. Energies are in kcal/mol.

Here, we rationalized the theoretical disagreement by interpreting the role of hydroxyl groups which were essentially overlooked in the previous studies[17,18] but abundantly exist in close proximity to the epoxide on GO surface.[22]

The chemisorbed OH preferentially sits on top of a carbon atom with the H pointing to the center of a hexagon. The rotation of O−H around the C−O axis with the O−H pointing from one to another nearby center of hexagon is barrierless. The binding energy and desorption barrier is 0.24 eV and 13.0 kcal/mol, respectively, indicating the singly chemisorbed OH is unstable and expected to dissociate at room temperature. The situation drastically changes until it finds a second OH or an epoxide in close proximity. To note, we took the same assumption as in ref 17 and 43 that oxygen groups were considered on the same side of the sheet since the formation of an epoxy line should be a one-side property.

Two hydroxyls adsorbed at the ortho (Figure 4a) or para (Figure 4c) positions form a nonmagnetic configuration because no unpaired electrons are present. It is noteworthy that, for both ortho and para positions, the binding of a subsequent OH is remarkably enhanced as compared to that in the singly adsorbed case. The para position is most favorable and the binding of a second OH is strongest among these three. The result is reasonable since two hydroxyls can form an H-bond which provides additional stability, and two oxygen atoms are not too close unlike the ortho case. The case with a second OH at the meta position (Figure 4b) which involves the creation of unpaired electrons gives the lowest binding energy. The migration barrier of OH from the meta to the ortho or para position is 15.9 and 12.6 kcal/mol, respectively, whereas the migration barrier of the reverse reaction is 49.1 and 52.8 kcal/mol, respectively, indicating that the second OH adsorbed at the meta position is unstable. We identified the reaction path leading to the formation of a water molecule and an epoxide remaining on the graphene surface from two hydroxyls adsorbed at the ortho or para positions (shown in Figure 5). Dually adsorbed OH can thus convert into one epoxide through the release of one water molecule if sufficient activation energy is given. The reverse reaction needs to overcome a much higher barrier (43.7 and 42.2 kcal/mol, respectively), implying that the dissociation of water near the epoxide does not easily occur.

The binding of OH is greatly strengthened with a nearby epoxide. As shown in Figure 6a, OH at S_2 gives the largest binding energy (1.18 eV) while the one at S_3 gives the smallest value (0.52 eV). The energy difference would be a combined effect of the H-bond and the ease of nucleophilic addition of OH radical to carbon. The desorption barriers for these two cases are 27.6 and 16.7 kcal/mol, respectively, indicating OH at S_2 is energetically more stable. The S_2 position should have the largest binding energy of OH due to the formation of a strong H-bond (H···O distance 2.03 Å). Though S_3 is nearer to the epoxide compared to S_4, the H···O distance for S_3 (S_4) increases to 2.87 Å (3.05 Å). The H-bond contribution is largely weakened. Therefore, we rationalized the binding energy difference between S_3 and S_4 by taking into account another factor, that is, the ease of nucleophilic addition of OH radical to carbon. OH at S_4 has a larger binding energy than that at S_3 which agrees with the carbon atomic charge difference ($\Delta Q = Q_{S4} - Q_{S3} = -0.05$ e) before the OH addition and the shorter C−O bond at S_4 after the addition. It is worthy to note, OH at S_2 also increases the binding of the epoxide by 0.84 eV. Our results agree well with the previous experimental work showing

dx.doi.org/10.1021/jp4052159 | J. Phys. Chem. C 2013, 117, 17832−17838

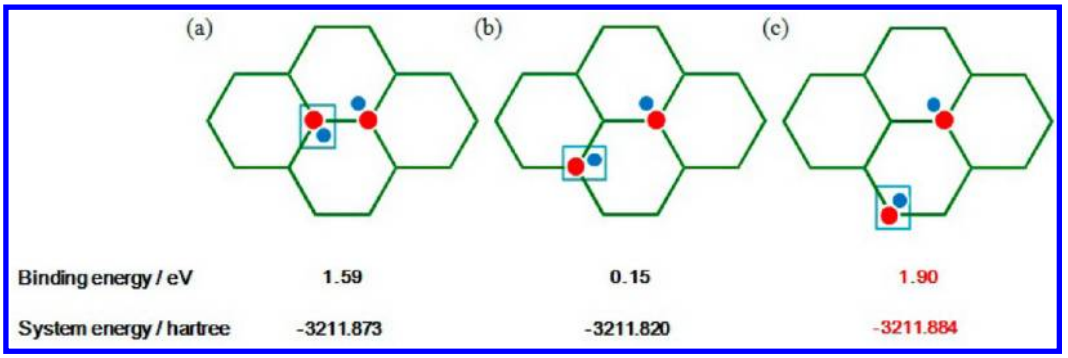

Figure 4. Binding energies of specified hydroxyls and system energies of tested configurations when two hydroxyls are coadsorbed at the ortho (a), meta (b), or para (c) positions of the same carbon hexagon of $C_{80}H_{22}$. The binding of subsequent OH is specified by a blue square.

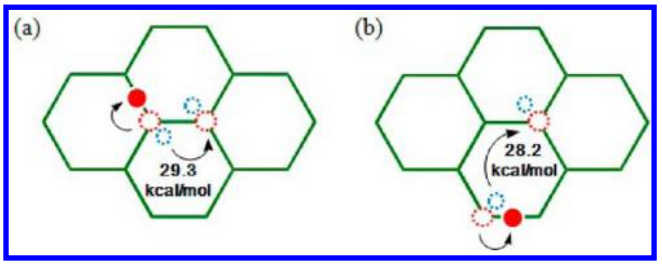

Figure 5. Reaction barriers for two hydroxyls at the ortho (a) or para (b) positions of the same carbon hexagon of $C_{80}H_{22}$ toward the release of a water molecule.

a large portion of C−OH and C−epoxide are bonded to each other on the GO surface.[22] But surprisingly, the jumping of the epoxide in the most favorable pair configuration has a barrier as low as 15.0 kcal/mol (Figure 6b) which is largely reduced compared to that in the isolated epoxide case (Figure 3a). Such a stark energy decrease would be ascribed to the H-bonding that "stabilizes" the epoxide migration. Compared to that of the direct hydrogen transfer forming a new hydroxyl-epoxide pair (Figure 6c), the barrier height is still lower by 9.3 kcal/mol.

The OH-facilitated epoxide migration could therefore be applicable to explain the oxygen line defect. Figure 7 displays the most feasible reaction scenarios taking account of the system stability. In the formation of a linear epoxide dimer, r_1 in Figure 7a bears the lowest barrier (only 11.5 kcal/mol) which is 3.5 and 17.4 kcal/mol lower than that in Figure 6b and Figure 3b, respectively, suggesting the linear epoxide dimerization is easily initiated if the ambient chemistry is satisfied. r_1 in Figure 7b has a barrier almost equal to that of R_1 in Figure 3b owing to the absence of H-bonding in the process of oxygen jumping. When two hydroxyls are covalently adsorbed on the same ring with an epoxide (Figure 7c), the second epoxide jumping requires 21.4 kcal/mol to proceed via r_1. The configurations

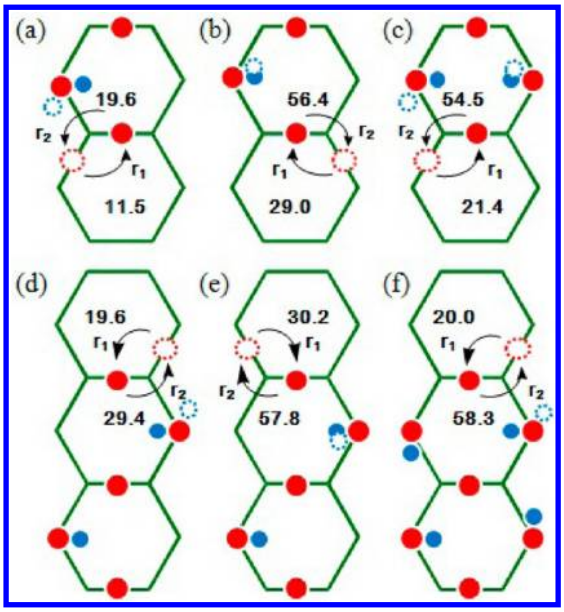

Figure 7. Oxygen hopping barriers toward the formation (r_1) or deformation (r_2) of the epoxy line in the presence of hydroxyls on $C_{80}H_{22}$. Energies are in kcal/mol.

having two or four interlaced OH were tested for the generation of a linear epoxide trimer. The system energy for two interlaced OH (Figure 7d) is lower than that with two OH which are inserted all-left or all-right, and the system energy for four clockwise distributed OH (Figure 7f) is lowest among the tested conformers. Though in Figure 7d the barrier for r_1 increases to 19.6 kcal/mol, it is still significantly lower than that without OH. Once the line forms, to trigger the H-transfer a much higher barrier (28.5 kcal/mol) needs to be overcome. Similar to the case in Figure 7b, the extension of the epoxy row

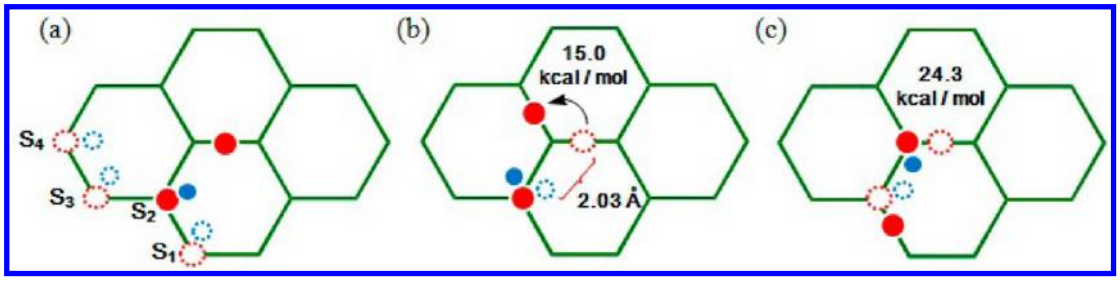

Figure 6. Possible configurations for the hydroxyl−epoxide pair when the two groups are close to each other (a), the barrier of the epoxide migration (b), and the direct H-transfer (c) in the most favorable pair configuration on $C_{80}H_{22}$. S_n (n = 1, 2, 3, 4) indicates the possible OH binding site.

dx.doi.org/10.1021/jp4052159 | J. Phys. Chem. C 2013, 117, 17832−17838

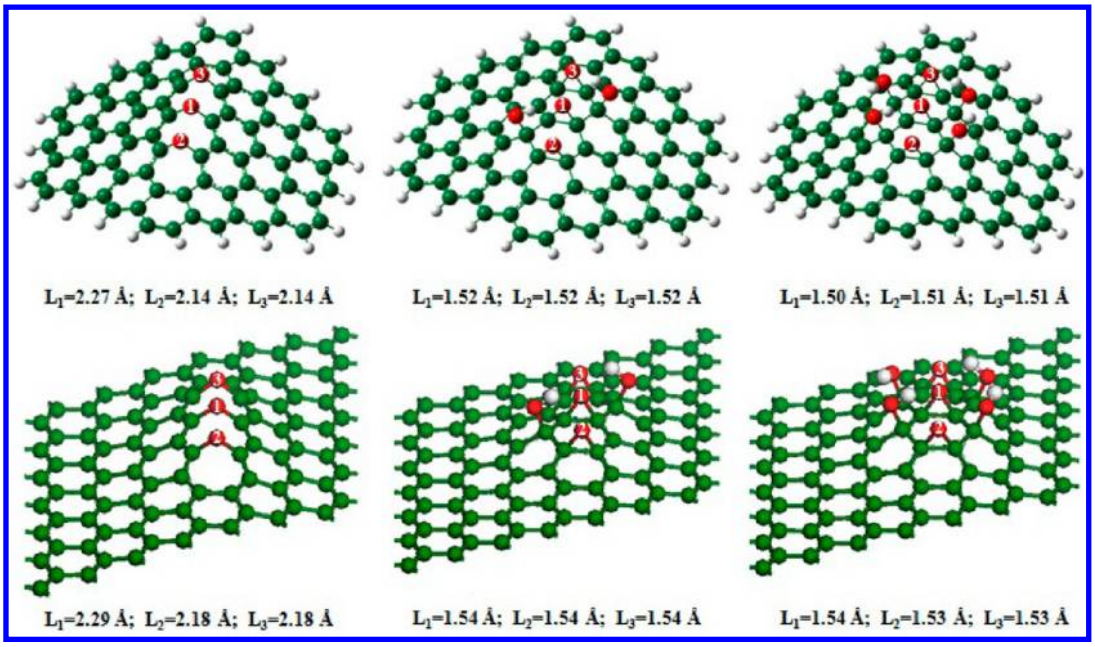

Figure 8. Structure and bond length changes upon intercalation of hydroxyls in the epoxy line. The first row refers to cases based on the graphene flake. The second row corresponds to cases based on the 7 × 7 × 1 graphene supercell. L_1, L_2, and L_3 denote the bond length of epoxy carbons.

in Figure 7e becomes more difficult because the H-bonding fails to mediate the oxygen migration. We also found a very special oxygen clustering (Figure 7f) that the minimum energy required to initiate the OH desorption is 41.3 kcal/mol which is the largest among our tested conformers. To trigger the H-transfer, the energy required is even larger (50.0 kcal/mol). The reverse reactions against the linear oxygen assembly are exclusively more difficult, especially when the sp^2 carbons are saturated with OH in the clustering. This clarifies once the epoxide is "locked" in a line it is less likely to move elsewhere. It is noteworthy that both finite and periodic calculations (Figure 8) illustrate that the intercalation of OH prevents the unzipping of underlying carbons and induces a smoother protrusion along the epoxy line. OH herein might act as a strain release center that partially releases the strain created by epoxy bridges.

The literature regarding oxygen diffusion on graphene surface, especially the comparison between experiment and theory, is very limited. Yang et al.[36] used etch-decoration transmission electron microscopy to obtain direct evidence for the surface diffusion of oxygen on graphite and an estimate of 35 kcal/mol for the activation energy of site-to-site hopping. The result (36.4 kcal/mol) obtained from our finite graphene flake is quantitative, but numerical agreement with experiment would be very surprising. We calculated the corresponding value (23.6 kcal/mol) under PBCs which turns out to be underestimated as compared to the experimental data. There are limitations associated with PBCs when used in conjunction with a relatively small GO sheet in the unit cell since the periodicity forces the overall graphene plane to be generally flat. If the sheet puckers significantly, PBCs will generate internal stresses as bonds are forced to stretch, which may not be realistic. Large unit cell and unit-cell optimization are therefore recommended but it does require significant additional computational cost. As shown in Figure 9, periodic calculations based on a 7 × 7 × 1 graphene supercell yield an overall trend of declined barriers compared to those obtained from $C_{80}H_{22}$, but both of the graphene models demonstrate the presence of OH lowers the epoxide migration barrier toward the formation

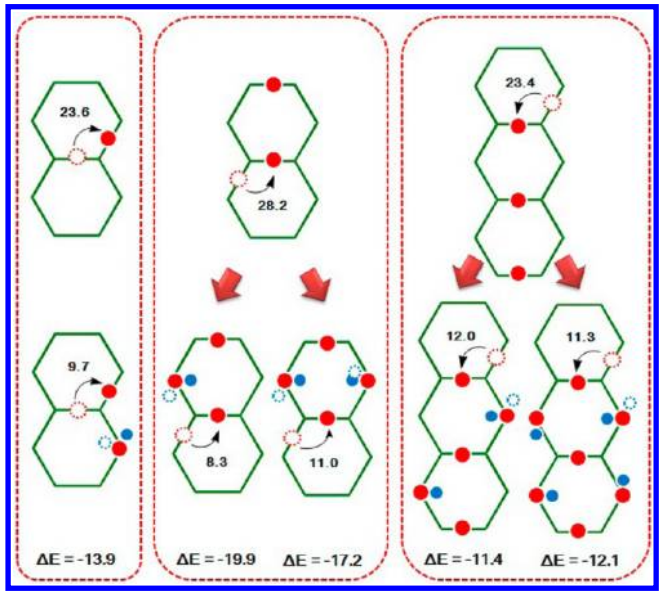

Figure 9. Oxygen hopping barriers in the presence or absence of hydroxyls under periodic boundary conditions. Energies are in kcal/mol.

of an epoxy line. Although the linear epoxide dimerization seems to be difficult which is somewhat different from the trend obtained from $C_{80}H_{22}$, the intercalation of OH reduces the barrier drastically, and as a result facilitates the migration. The mismatch would be ascribed to the extra flexibility and structure deformation allowed by the graphene flake.

CONCLUSIONS

In the process of graphite oxidation, oxygens which eventually constitute the epoxy line may come from two sources: (1) the directional binding of new epoxides; (2) the migration of existing epoxides to designated locations. Since a well-defined epoxy line on the graphene surface is not observed under the environment of atomic oxygens,[23] we thus infer such a defective

dx.doi.org/10.1021/jp4052159 | J. Phys. Chem. C 2013, 117, 17832−17838

line would preferentially grow via the migration of existing epoxides assisted by hydroxyls, rather than directly form due to strong oxidizing agents. PCM calculations manifest that solvents such as water or dimethylformamide can reduce the single epoxide hopping barrier by ca. 8 kcal/mol so that the migration of isolated epoxide which is away from the aggregation center can be facilitated. Once the hydroxyl-epoxide line forms, it induces a smooth surface buckling along the line without breaking the underlying carbon bonds which may shed light on the observation of ripples in suspended graphene monolayers. The hydroxyl-epoxide lines of GO might also be responsible for its much smaller size compared with the starting graphene during thermal reduction as molecular dynamics simulations[44] revealed that the removal of carbons from the graphene plane is more likely to occur when the initial hydroxyl and epoxy groups are close to each other. The calculations for periodic systems based on a $7 \times 7 \times 1$ graphene supercell give an overall trend of declined barriers in comparison to those obtained from the model flake, but identically the presence of OH lowers the epoxide migration barrier toward the formation of an epoxy line. Given that the previous reports[17,18] did not consider the participation of hydroxyls in surface-group rearrangements, further experimental work would thus be indispensable to confirm the presence or absence of the identified mechanism for the generation of oxygen line defects on these materials.

AUTHOR INFORMATION

Corresponding Author

*Jin Yong Lee Department of Chemistry, Sungkyunkwan University, 2066 Seobu-Ro, Jangan-Gu, Suwon 440-746, Korea. Tel: (82) 31-299-4560. E-mail: jinylee@skku.edu.

Notes

The authors declare no competing financial interest.

ACKNOWLEDGMENTS

Contract/grant sponsor: National Research Foundation of Korea through Contract/Grant No. 2007-0056343 and 2011-0015757. Contract/grant sponsor: KISTI Supercomputing Center (through the strategic support program for the supercomputing application research) through Contract/Grant No. KSC-2011-C2-54. Contract/grant sponsor: Ministry of Science, ICT & Future Planning (Project EDISON) through Contract/Grant No. 2012M3C1A6035359.

REFERENCES

(1) Novoselov, K. S.; Geim, A. K.; Morozov, S. V.; Jiang, D.; Zhang, Y.; Dubonos, S. V.; Grigorieva, I. V.; Firsov, A. A. Electric Field Effect in Atomically Thin Carbon Films. *Science* **2004**, *306*, 666−669.

(2) Zhang, Y.; Tan, Y. W.; Stormer, H. L.; Kim, P. Experimental Observation of the Quantum Hall Effect and Berry's Phase in Graphene. *Nature* **2005**, *438*, 201−204.

(3) Castro Neto, A. H.; Guinea, F.; Peres, N. M. R.; Novoselov, K. S.; Geim, A. K. The Electronic Properties of Graphene. *Rev. Mod. Phys.* **2009**, *81*, 109−162.

(4) Hirsch, A. The Era of Carbon Allotropes. *Nat. Mater.* **2010**, *9*, 868−871.

(5) Yu, S. U.; Cho, Y.; Park, B.; Kim, N.; Youn, I. S.; Son, M.; Kim, J. K.; Choi, H. C.; Kim, K. S. Fast Benchtop Visualization of Graphene Grain Boundaries Using Adhesive Properties of Defects. *Chem. Commun.* **2013**, *49*, 5474−5476.

(6) Kemp, K. C.; Seema, H.; Saleh, M.; Le, N. H.; Mahesh, K.; Chandra, V.; Kim, K. S. Environmental Applications Using Graphene Composites: Water Remediation and Gas Adsorption. *Nanoscale* **2013**, *5*, 3149−3171.

(7) Chandra, V.; Yu, S. U.; Kim, S. H.; Yoon, Y. S.; Kim, D. Y.; Kwon, A. H.; Meyyappan, M.; Kim, K. S. Highly Selective CO_2 Capture on N-Doped Carbon Produced by Chemical Activation of Polypyrrole Functionalized Graphene Sheets. *Chem. Commun.* **2012**, *48*, 735−737.

(8) Yang, J. W.; Lee, G.; Kim, J. S.; Kim, K. S. Gap Opening of Graphene by Dual Fecl3-Acceptor and K-Donor Doping. *J. Phys. Chem. Lett.* **2011**, *2*, 2577−2581.

(9) Park, J.; Lee, W. H.; Huh, S.; Sim, S. H.; Kim, S. B.; Cho, K.; Hong, B. H.; Kim, K. S. Work-Function Engineering of Graphene Electrodes by Self-Assembled Monolayers for High-Performance Organic Field-Effect Transistors. *J. Phys. Chem. Lett.* **2011**, *2*, 841−845.

(10) Min, S. K.; Kim, W. Y.; Cho, Y.; Kim, K. S. Fast DNA Sequencing with a Graphene-Based Nanochannel Device. *Nat. Nanotechnol.* **2011**, *6*, 162−165.

(11) Chandra, V.; Park, J.; Chun, Y.; Lee, J. W.; Hwang, I. C.; Kim, K. S. Water-Dispersible Magnetite-Reduced Graphene Oxide Composites for Arsenic Removal. *Acs Nano* **2010**, *4*, 3979−3986.

(12) Kim, K. S.; Zhao, Y.; Jang, H.; Lee, S. Y.; Kim, J. M.; Kim, K. S.; Ahn, J. H.; Kim, P.; Choi, J. Y.; Hong, B. H. Large-Scale Pattern Growth of Graphene Films for Stretchable Transparent Electrodes. *Nature* **2009**, *457*, 706−710.

(13) Kim, W. Y.; Kim, K. S. Prediction of Very Large Values of Magnetoresistance in a Graphene Nanoribbon Device. *Nat. Nanotechnol.* **2008**, *3*, 408−412.

(14) Becerril, H. A.; Mao, J.; Liu, Z.; Stoltenberg, R. M.; Bao, Z.; Chen, Y. Evaluation of Solution-Processed Reduced Graphene Oxide Films as Transparent Conductors. *ACS Nano* **2008**, *2*, 463−470.

(15) Gomez-Navarro, C.; Meyer, J. C.; Sundaram, R. S.; Chuvilin, A.; Kurasch, S.; Burghard, M.; Kern, K.; Kaiser, U. Atomic Structure of Reduced Graphene Oxide. *Nano Lett.* **2010**, *10*, 1144−1148.

(16) Dreyer, D. R.; Park, S.; Bielawski, C. W.; Ruoff, R. S. The Chemistry of Graphene Oxide. *Chem. Soc. Rev.* **2010**, *39*, 228−240.

(17) Li, J. L.; Kudin, K. N.; McAllister, M. J.; Prud'homme, R. K.; Aksay, I. A.; Car, R. Oxygen-Driven Unzipping of Graphitic Materials. *Phys. Rev. Lett.* **2006**, *96*, 176101.

(18) Ajayan, P. M.; Yakobson, B. I. Materials Science—Oxygen Breaks into Carbon World. *Nature* **2006**, *441*, 818−819.

(19) Pei, S. F.; Cheng, H. M. The Reduction of Graphene Oxide. *Carbon* **2012**, *50*, 3210−3228.

(20) Schniepp, H. C.; Kudin, K. N.; Li, J. L.; Prud'homme, R. K.; Car, R.; Saville, D. A.; Aksay, I. A. Bending Properties of Single Functionalized Graphene Sheets Probed by Atomic Force Microscopy. *ACS Nano* **2008**, *2*, 2577−2584.

(21) Gao, W.; Alemany, L. B.; Ci, L. J.; Ajayan, P. M. New Insights into the Structure and Reduction of Graphite Oxide. *Nat. Chem.* **2009**, *1*, 403−408.

(22) Cai, W. W.; Piner, R. D.; Stadermann, F. J.; Park, S.; Shaibat, M. A.; Ishii, Y.; Yang, D. X.; Velamakanni, A.; An, S. J.; Stoller, M.; et al. Synthesis and Solid-State NMR Structural Characterization of ^{13}C-Labeled Graphite Oxide. *Science* **2008**, *321*, 1815−1817.

(23) Hossain, M. Z.; Johns, J. E.; Bevan, K. H.; Karmel, H. J.; Liang, Y. T.; Yoshimoto, S.; Mukai, K.; Koitaya, T.; Yoshinobu, J.; Kawai, M.; et al. Chemically Homogeneous and Thermally Reversible Oxidation of Epitaxial Graphene. *Nat. Chem.* **2012**, *4*, 305−309.

(24) Lee, G. D.; Wang, C. Z.; Yoon, E.; Hwang, N. M.; Kim, D. Y.; Ho, K. M. Diffusion, Coalescence, and Reconstruction of Vacancy Defects in Graphene Layers. *Phys. Rev. Lett.* **2005**, *95*, 205501.

(25) Ding, F.; Jiao, K.; Lin, Y.; Yakobson, B. I. How Evaporating Carbon Nanotubes Retain Their Perfection? *Nano Lett.* **2007**, *7*, 681−684.

(26) Miyawaki, J.; Yuge, R.; Kawai, T.; Yudasaka, M.; Iijima, S. Evidence of Thermal Closing of Atomic-Vacancy Holes in Single-Wall Carbon Nanohorns. *J. Phys. Chem. C* **2007**, *111*, 1553−1555.

(27) Tsetseris, L.; Pantelides, S. T. Adatom Complexes and Self-Healing Mechanisms on Graphene and Single-Wall Carbon Nanotubes. *Carbon* **2009**, *47*, 901−908.

(28) Psofogiannakis, G. M.; Froudakis, G. E. DFT Study of Hydrogen Storage by Spillover on Graphite with Oxygen Surface Groups. *J. Am. Chem. Soc.* **2009**, *131*, 15133−15135.
(29) Gao, X. F.; Jang, J.; Nagase, S. Hydrazine and Thermal Reduction of Graphene Oxide: Reaction Mechanisms, Product Structures, and Reaction Design. *J. Phys. Chem. C* **2010**, *114*, 832−842.
(30) Liu, H.; Lee, J. Y. Electric Field Effects on the Adsorption of CO on a Graphene Nanodot and the Healing Mechanism of a Vacancy in a Graphene Nanodot. *J. Phys. Chem. C* **2012**, *116*, 3034−3041.
(31) Frisch, M. J.; Trucks, G. W.; Schlegel, H. B.; Scuseria, G. E.; Robb, M. A.; Cheeseman, J. R.; Scalmani, G.; Barone, V.; Mennucci, B.; Petersson, G. A. et al. *Gaussian 09*, revision B.01; Gaussian Inc.: Wallingford CT, 2010.
(32) Zhao, Y.; Truhlar, D. G. The M06 Suite of Density Functionals for Main Group Thermochemistry, Thermochemical Kinetics, Noncovalent Interactions, Excited States, and Transition Elements: Two New Functionals and Systematic Testing of Four M06-Class Functionals and 12 Other Functionals. *Theor. Chem. Acc.* **2008**, *120*, 215−241.
(33) Zhao, Y.; Truhlar, D. G. Density Functionals with Broad Applicability in Chemistry. *Acc. Chem. Res.* **2008**, *41*, 157−167.
(34) Wheeler, S. E.; Houk, K. N. Integration Grid Errors for Meta-GGA-Predicted Reaction Energies: Origin of Grid Errors for the M06 Suite of Functionals. *J. Chem. Theory Comput.* **2010**, *6*, 395−404.
(35) Liu, H.; Lee, J. Y. Electric Field Assisted Oxygen Removal from the Basal Plane of the Graphitic Material. *J. Comput. Chem.* **2013**, *34*, 305−310.
(36) Yang, R. T.; Wong, C. Kinetics and Mechanism of Oxidation of Basal Plane on Graphite. *J. Chem. Phys.* **1981**, *75*, 4471−4476.
(37) Cossi, M.; Scalmani, G.; Rega, N.; Barone, V. New Developments in the Polarizable Continuum Model for Quantum Mechanical and Classical Calculations on Molecules in Solution. *J. Chem. Phys.* **2002**, *117*, 43−54.
(38) Lin, Z. Y.; Yao, Y. G.; Li, Z.; Liu, Y.; Li, Z.; Wong, C. P. Solvent-Assisted Thermal Reduction of Graphite Oxide. *J. Phys. Chem. C* **2010**, *114*, 14819−14825.
(39) Delley, B. From Molecules to Solids with the DMol3 Approach. *J. Chem. Phys.* **2000**, *113*, 7756−7764.
(40) Hammer, B.; Hansen, L. B.; Norskov, J. K. Improved Adsorption Energetics within Density-Functional Theory Using Revised Perdew−Burke−Ernzerhof Functional. *Phys. Rev. B* **1999**, *59*, 7413−7421.
(41) Halgren, T. A.; Lipscomb, W. N. The Synchronous-Transit Method for Determining Reaction Pathways and Locating Molecular Transition States. *Chem. Phys. Lett.* **1977**, *49*, 225−232.
(42) Suarez, A. M.; Radovic, L. R.; Bar-Ziv, E.; Sofo, J. O. Gate-Voltage Control of Oxygen Diffusion on Graphene. *Phys. Rev. Lett.* **2011**, *106*, 146802.
(43) Schniepp, H. C.; Li, J. L.; McAllister, M. J.; Sai, H.; Herrera-Alonso, M.; Adamson, D. H.; Prud'homme, R. K.; Car, R.; Saville, D. A.; Aksay, I. A. Functionalized Single Graphene Sheets Derived from Splitting Graphite Oxide. *J. Phys. Chem. B* **2006**, *110*, 8535−8539.
(44) Bagri, A.; Mattevi, C.; Acik, M.; Chabal, Y. J.; Chhowalla, M.; Shenoy, V. B. Structural Evolution during the Reduction of Chemically Derived Graphene Oxide. *Nat. Chem.* **2010**, *2*, 581−587.